Filtering of SPECT Reconstructions Made Using Bellini's Attenuation Correction Method: a Comparison of Three Pre-Reconstruction Filters and a Post-Reconstruction Wiener Filter.

Stephen J. Glick, Bill C. Penney, Michael A. King
Department of Nuclear Medicine, University of Massachusetts Medical Center
Worcester, MA 01655

Abstract

This study evaluates a three-dimensional (3D) Wiener filter which is used to restore SPECT reconstructions which were made using Bellini's method of attenuation correction. Its performance is compared to that of several pre-reconstruction filters: 1) the one-dimensional (1D) Butterworth, 2) the two-dimensional (2D) Butterworth, and 3) a 2D Wiener filter. A simulation study is used to compare the four filtering methods. An approximation to a clinical liver spleen study was used as the source distribution and an algorithm which accounts for the depth and distance dependent blurring in SPECT was used to compute noise free projections. To study the effect of filtering method on tumor detection accuracy, a 2cm diameter, "cool" spherical tumor (40% contrast) was placed at a known, but random, location within the liver. Projection sets for ten tumor locations were computed and five noise realizations of each set were obtained by introducing Poisson noise. The simulated projections were either: 1) filtered with the 1D or 2D Butterworth or the 2D Wiener and then reconstructed using Bellini's intrinsic attenuation correction, or 2) reconstructed first, then filtered with the 3D Wiener. The criteria used for comparison were: 1) normalized mean square error (NMSE), 2) cold spot contrast, and 3) accuracy of tumor detection with an automated numerical method. Results indicate that restorations obtained with 3D Wiener filtering yielded significantly higher lesion contrast and lower NMSE values compared to the other methods of processing. The Wiener restoration filters and the 2D Butterworth all provided similar measures of detectability, which were noticeably higher than that obtained with 1D Butterworth smoothing.

I. INTRODUCTION

In single photon emission computed tomography (SPECT), the reconstructions are blurred in all directions by the effects of scatttered radiation, septal penetration, the collimator and detector response and the reconstruction process. Furthermore, the reconstructed slices can yield a higher fractional standard deviation than in a single planar image with the same count level. Stationary restoration filtering can be used to partially compensate for the sources of three-dimensional (3D) blur, while also suppressing noise [1,2]. The restoration filter can be applied to the reconstructed data (3D post-reconstruction filtering) or to the projection images before reconstruction (two-dimensional (2D) pre-reconstruction filtering).

There are a number of reasons why 3D post-reconstruction restoration filtering might be preferred to 2D pre-reconstruction filtering. In stationary restoration filtering, a linear shift-invariant imaging system is assumed. Investigations have shown that in a uniform attenuation medium, both the 2D modulation transfer function (MTF) (pre-reconstruction) and the 3D MTF (post-reconstruction) of SPECT vary with position, especially at locations closer to the body outline [3]. It has also been noted that reconstructing with intrinsic attenuation correction as described by Bellini *et.al.* [4] yields a 3D MTF which varies less with position within the transverse slices than the combined conjugate view 2D MTF varies with depth [5]. Thus the assumption of shift invariance used in stationary restoration filtering becomes less of an approximation for 3D post- than for 2D pre-reconstruction restoration filtering. Other possible advantages of 3D post-reconstruction filtering include: 1) the initial reconstruction can be used to provide a good estimate of the object power spectrum needed in forming an image-dependent filter, 2) the 3D MTF used in 3D filtering includes the effects of the reconstruction process and attenuation correction, 3) a 3D filter can be anisotropic in all three directions, and 4) post-reconstruction filtering can be applied to fan or cone beam reconstructions.

In this study a newly developed method of image-dependent, 3D post-reconstruction Wiener filtering of SPECT images [6] is compared to: 1) 2D pre-reconstruction Wiener filtering, and 2) one-dimensional (1D) and 2D But-

This work was supported by the National Cancer Institute under grant CA-42165.

0018-9499/91/0400-0663$01.00 © 1991 IEEE

terworth smoothing of the projection images. To compare the different filtering methods a simulated clinical liver spleen study was developed. A 3D analytical simulation of SPECT imaging was then used to generate a number of simulated projection image sets, where a 2cm diameter, 40% contrast, "cool" spherical tumor was randomly placed in the liver of each set. Poisson noise was added to the projection data to create five noise realizations of each set. These projections were either processed with one of the pre-reconstruction filters and then reconstructed with Bellini's attenuation correction method, or reconstructed first, and then processed with the 3D Wiener. The figures-of-merit that were used to compare the different filtering methods included: 1) image fidelity as assessed by the normalized mean square error (NMSE), 2) cold spot contrast, and 3) a technique for numerical assessment of tumor detection accuracy.

II. METHODS

Wiener restoration uses the optimality criterion of minimizing the mean squared error between the restored image and the original object. Its derivation assumes that both the object and noise can be modelled as stationary independent random processes. Such assumptions are made in this study. The Wiener filter, which can be formulated in the frequency domain as:

$$W(f) = MTF(f)/[MTF(f)^2 + N(f)^2/B(f)^2], \qquad (1)$$

requires an estimate of several functions, namely: 1) the MTF of the imaging system, 2) the expected value of the power spectrum of the noise process (N^2), and 3) the power spectrum of the random process of which the object is assumed to be a sample (B^2). The Wiener filter formulation given in eq. (1) can be represented as a function of multidimensional frequency (f). In this paper, the components of f will be denoted u,v, and w, which are the frequency domain coordinates corresponding to the horizontal, vertical, and axial directions, respectively.

A. 2D Wiener filter

The methods used to estimate MTF, N^2, and B^2 for the 2D Wiener filter are described elsewhere [7]. Since the estimates of these functions are all isotropic, the resulting 2D filter is also isotropic. The same filter is then used on each combined conjugate view projection image (the filter does not vary with angle).

B. 3D Wiener filter

The 3D Wiener filter used is based on a rearrangement of eq. (1) given by Madsen *et.al.* [8]. In his formulation, the Wiener filter is expressed as:

$$W(f) = (1/MTF^2)[MTF^2(f)B^2(f)/(MTF^2(f)B^2(f) + N^2(f)). \qquad (2)$$

The advantage of this formulation is that it avoids the necessity of estimating B^2. Instead, the power spectrum of the blurred object (MTF^2B^2) is estimated. In addition to this function, the MTF and N^2 must also be estimated. The methods used are briefly discussed below.

In a comparison of several attenuation correction methods, it was determined that intrinsic attenuation correction as described by Bellini *et.al.*, significantly reduces the position dependence of the 3D MTF [5]. However, the spatial resolution of the point spread function in the projection plane varies with source distance from the collimator face. Also the contribution of scattered radiation to the projection image varies with angle (because the depth and position of the source varies with viewing direction). Thus, the reconstructed 3D MTF still varies with position, especially at locations near the edge of the body outline. Therefore, an "effective" 3D MTF was formed by averaging the 3D MTFs obtained for locations mid-way between the center and edge along the minor and major axes of the elliptical body outline.

Simulation studies were used to characterize the tomographic 3D noise power spectrum (N^2) associated with Bellini's attenuation correction method. The standard object used was a 30x23cm cylinder with uniformly distributed activity. An activity distribution which approximated a clinical liver spleen study was also used. A 3D non-stationary simulation of SPECT imaging [9,10] (described below) was used to create a 64x64 pixel projection image set consisting of 128 projection angles. This noise-free projection set was scaled to contain 50,000 counts/frame on the average. Fifty noisy projection sets were created by introducing independent Poisson noise into the noise-free projection set. Each of the 50 noisy projection sets, and the noise-free set, were reconstructed using Bellini's method and filtered backprojection (with a ramp filter). Each noisy 3D reconstruction was subtracted from the noise-free reconstruction, and the power spectrum of each 3D difference set was calculated. The individual power spectra were then averaged to reduce the error in the resulting N^2 estimate. This procedure was also performed for 30cm diameter circular and 30x15cm elliptical cross-sectional body outlines. Since Bellini's method and filtered backprojection operate on each slice independently, the noise is uncorrelated in the axial direction. This allowed the 3D noise spectra obtained from these simulations to be averaged in the axial direction, resulting in a 2D function. Averaging the results from 50 simulations with independent noise reduced the standard deviation of the individual N^2 terms by a factor of roughly 57 (the square root of (64 x 50)).

Thus, a low variance estimate of the shape of N^2 was available. To estimate the magnitude of N^2 in the reconstruction which is to be 3D Wiener filtered, the blurred object spectrum is assumed negligible compared to the noise in the peri-Nyquist frequency range (those frequencies near the Nyquist frequency) [11]. With this assumption, the average magnitude of the power spectrum of the reconstruction in the peri-Nyquist frequency range should equal the average magnitude of N^2 in this region. This relationship was used to appropriately scale the 2D estimated noise spectrum to estimate N^2 for the 3D Wiener filter.

The 3D blurred object spectrum was then estimated from the power spectrum of the particular reconstruction (G^2). Different methods were used to estimate the low versus the mid- to high-frequency range of this spectrum. At low frequencies, the difference between smoothed versions of G^2 and N^2 was used to estimate MTF^2B^2. At mid- to high-frequencies, a curve fitting procedure based on a power law equation for B^2 was used to estimate MTF^2B^2. The details of this procedure are being reported elsewhere [6].

Since the three functions used in computing the 3D Wiener filter can all be anisotropic, the filter can also be anisotropic.

C. 1D and 2D Butterworth filtering

The Butterworth filter (either 1D or 2D) was used to assess the difference in performance between a typical filter used in SPECT imaging and the 2D and 3D Wiener filters. The frequency domain Butterworth filter can be formulated as [12],

$$B(f) = 1/[1 + (f/f_c)^{2N}], \qquad (2)$$

where f_c is the cut-off frequency, and N is the order of the filter. In this study f_c was chosen to be .4 times the Nyquist frequency, and the order of the filter was chosen to be 4. These parameters were obtained from those recommended in the literature [13,14].

D. Simulation studies

A 3D analytical, non-stationary simulation [9,10] was used to create projection images. A mathematical approximation to a clinical Tc-99m liver spleen study provided the basis for the projection data. This model was obtained by fitting a set of ellipses to the boundaries of the liver and spleen in a clinical SPECT image. The subroutine PHAN of the RECLBL software package [15] was then used to create a 64x64x64 voxel set which was used as the true image. To minimize errors due to aliasing, the analytically defined truth was sampled using 10x10x10 sub-voxels per voxel. The 1000 sub-voxels were then averaged to obtain the resulting activity in the corresponding whole voxel. The non-stationary projection algorithm which was used to create the projection images was based on a serial model of the system transfer function and has been described elsewhere [9,10].

In order to compare the performance of the four filters in terms of tumor detectability, tumor contrast, and fidelity of the reconstruction, the following experiment was conducted. A computer program was developed to randomly generate the center location of two, 2cm diameter spheres positioned in the liver. These locations were subject to the constraint that the outer surface of the tumor sphere be twice the full width at half maximum (FWHM) (of the imaging system) from the boundary of the liver. Ten sets of two locations of the spheres were determined, where one location was selected to be a tumor site and one was selected as a "background" site (in this paper, the background location will be called a sham tumor site). By using a number of simulation studies with randomly chosen tumor locations, the experiment yields a detectability measurement which is unaffected by any position dependent degrading effects (*e.g.*, attenuation). For each of the ten tumor sites a 2cm diameter "cool" spherical tumor (40% contrast) was subtracted from the liver, and a 128 angle, 64x64 pixel, SPECT acquisition set with an average of 20,000 counts per frame was obtained. Five independent Poisson noise sets of each of the 10 noise-free projection image sets were created. Thus 50 simulated acquisitions containing 50 tumor sites and 50 sham tumor sites were available to conduct a study of tumor detection. These simulated projection image sets were then either: 1) filtered with one of the pre-reconstruction filters (1D or 2D Butterworth or 2D Wiener) and reconstructed using Bellini's attenuation correction method, or 2) reconstructed first, then filtered with the 3D Wiener.

To study the tumor detectability of the filtered SPECT images, the task to be performed was defined to be the detection of a cool tumor, given that the location of a possible tumor is known *a priori*. The decision variable used was the average value of voxels inside the non-blurred tumor (or sham tumor) region. This is an approximation to the matched filter, and has been previously used in a similar study by Hanson [16]. For each filtered image set, the decision variable was calculated for both the tumor and sham tumor regions. To determine the true positive fractions (TPFs) and true negative fractions (TNFs) needed to construct a receiver operator characteristic (ROC) curve, the following procedure was used. The TPFs were computed by determining the number of true tumor decision variable values which were greater than or equal to a selected threshold. The TNFs were computed by determining the number of sham tumor decision variable values falling below the same threshold. The

threshold values actually used were the values of the decision variables in both the true and the sham tumor sites. The resultant 100 (TPF,TNF) pairs were used to construct the ROC curve for each filtering method. The area under each ROC curve, which is the fracti n of correct answers obtained in the binary tumor detection task, was then computed using these 100 (TPF,TNF) pairs.

The tumor contrast was calculated using the formula $[N_T(\text{tumor site}) - N_T(\text{sham tumor site})] / N_T(\text{sham tumor site})$, where N_T is the average value of voxels inside the non-blurred tumor or sham tumor region. The average tumor contrast for each filter was obtained for the 50 reconstructions. The normalized mean square error (NMSE) between the true image and the filtered reconstruction was also calculated as a measure of fidelity.

III. RESULTS AND DISCUSSION

Figure 1 shows the u and v frequency axes of the Bellini noise power spectrum. It can be observed that it is anisotropic and varies minimally with the different source distributions (i.e., a uniform source distribution vs. a distribution which is an approximation to a clinical liver spleen). The shape of the noise power spectrum was also found to be heavily dependent on the outline of the attenuator.

Typical filter curves for each of the four methods are displayed in Fig. 2. Since the 2D pre-reconstruction filters are isotropic, they can be represented using 1D plots. The 3D Wiener filter is anisotropic and thus the filter values along the u,v, and w frequency axes are shown (bottom, Fig. 2).

The 2D Wiener filter used in this study differs in several ways from the 2D Wiener filter used in previous studies reported by our group [2,7]. The previous studies used only 64 projection angles, each with an average of 40,000-50,000 counts. The current study used 128 projections, each with an average of 20,000 counts. The source distribution used previously contained only a liver, spleen, and a diffuse "background" throughout the remainder of the body outline. The source distribution used in this study contained the liver and spleen, but the "background" was removed and the uptake of Tc-99m in the spine was roughly simulated. The changes made to the source distribution provided better agreement between the power spectrum of the simulated liver and spleen and that from clinical studies. These changes were primarily responsible for increasing the peak value of the 2D Wiener filter (Fig. 2) compared to that noted in a previous study [2]. The 2D Wiener filter used in this and previous studies did not adapt to the number of projection angles. Thus, different filters would be computed for a 64 view study with an average of 40,000 counts/view versus a 128 view study with 20,000 counts/view. It appears possible to compute a 2D Wiener filter for a standard number f views, given the actual number of views and th average counts/view. However, it is unclear what criterion should be used to determine the standard number of views to use. We have previously reported that the number of views affects the reconstructi n obtained, given that the same total counts in the acquisition set is maintained [17].

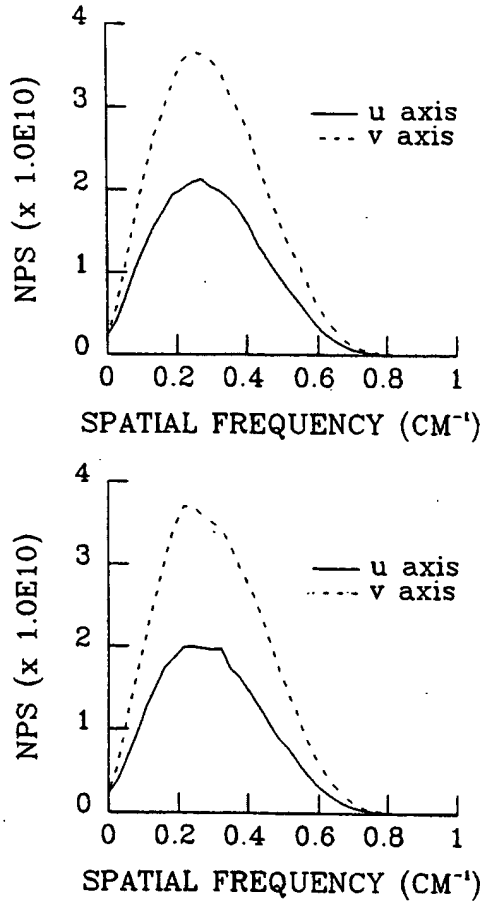

Figure 1. Shown here are the values along the u and v spatial frequency axes of the tomographic noise power spectrum (NPS) obtained with Bellini's attenuation correction method. Two different activity distributions were used in a 30x23cm cylindrical body outline. The plot on the top shows the NPS corresponding to a uniformly distributed activity, and the plot on the bottom shows that for an activity distribution which approximates a clinical liver spleen study.

Figure 3 shows a transverse slice through the liver and spleen for: a) the "truth", b) the reconstruction obtained with no filtering, c) the reconstruction obtained with 1D Butterworth smoothing, d), that obtained with 2D Butterworth smoothing, e) that obtained with 2D Wiener restoration, and

f) that obtained with 3D Wiener restoration. Notice that the slice obtained with 3D Wiener restoration appears to show the least artifact in the background area between the liver and spleen. Fig. 4 displays a profile through the liver and spleen for each of the images shown in Fig. 3. It can be observed that the profile of the slices obtained with the restoration filters are closer to the true profile than those obtained with no processing or the smoothing filters. From both the images (Fig. 3) and the profiles (Fig. 4), it can be observed that the restoration filters yield a hot rim artifact around the liver. This rim overshoot is characteristic of restoration filtered images and is related to the rapidity of the decrease from its peak value down toward zero as the radial frequency increases. Techniques for minimizing this artifact deserve further study.

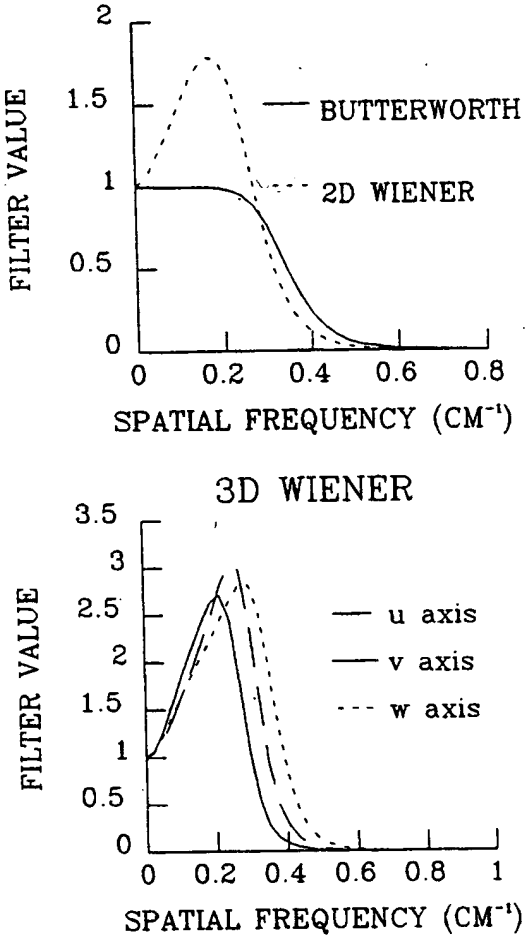

Figure 2. Comparison of typical filter functions applied to the simulated SPECT liver spleen study. Both the Butterworth (1D and 2D are the same) and 2D Wiener are shown on the top, and the three frequency axes of the 3D Wiener filter are shown below.

As seen in Table I, the NMSE values for the 2D and 3D Wiener restoration methods were similar (7.9% and 6.0%), and distinctly lower than for 1D and 2D Butterworth smoothing (12.8% and 12.6%). The slightly better NMSE values obtained with the 3D Wiener filter might have been due to: 1) the allowance f the 3D Wiener filter to vary in all directions whereas the 2D Wiener was forced to be isotropic, 2) including the influence of attenuation and the reconstruction process in the 3D MTF, and 3) the ability of the 3D filter to adapt to the number of counts in the study. The average cold spot contrast, expressed as a percent of the true tumor contrast (40%) is reported in Table I. The restorations obtained with the 3D Wiener filter had a higher tumor contrast (25%) than the other processing methods, but it also had a high standard deviation of the contrast (approximately equal to that obtained with the 1D Butterworth). The higher contrast obtained with the 3D Wiener filter might be attributable to both over and undershooting which occurs in areas of high activity change.

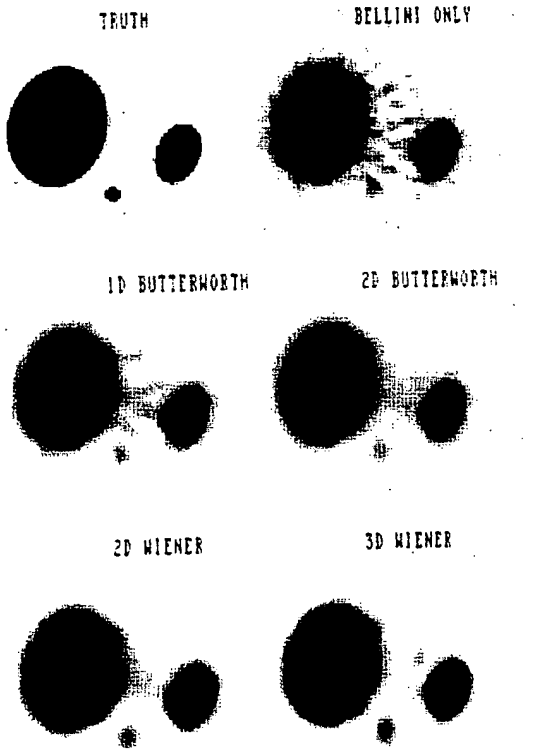

Figure 3. Reconstructed slices through the liver and spleen. Shown are the "true" slice, the reconstructed slice with no filtering, and the reconstructed slice obtained with each of the four filtering methods. Bellini's attenuation correction has been used in all of the reconstructions. It can be observed that slices obtained with the restoration filters have less artifact in the background area between the liver and spleen.

The area under the receiver operator characteristic curves (ROC) for the four filtering methods are also shown in Table I. The Wiener restoration filters and the 2D Butterworth filter all provided similar measures of detectability (area under the ROC curve). These values were higher (6-8%) than that btained with 1D Butterworth smoothing. This result agrees with a previous study [1] and visual observations which suggest that significant improvement in image quality can be obtained by including interslice information into the filtering process (i.e., by performing either 2D pre-reconstruction filtering of the projection images or 3D post-reconstruction filtering of the slices).

The clinical implications of this study need to be examined cautiously, however, because the decision variable used has not been shown to correlate with tumor detection performance of the human observer. It has been noted that deconvolution of long-tailed point spread functions (*e.g.*, those for scattered radiation) improves the detection task performance of human observers but does not improve the performance of several aut mated detectors [18,19]. Hence, the comparison between Butterworth smoothing and restoration filtering given herein may not accurately reflect their effects on tumor detection accuracy by human observers. Clearly, tumor detection studies with human observers would be required to definitively compare the different processing methods. The difference in ROC area noted for 1D Butterworth smoothing and 2D Wiener restoration is substantial (0.75 vs. 0.83 respectively). Since 1D Butterworth smoothing is in wide clinical use, a comparison of these methods using human observer ROC studies may be warranted.

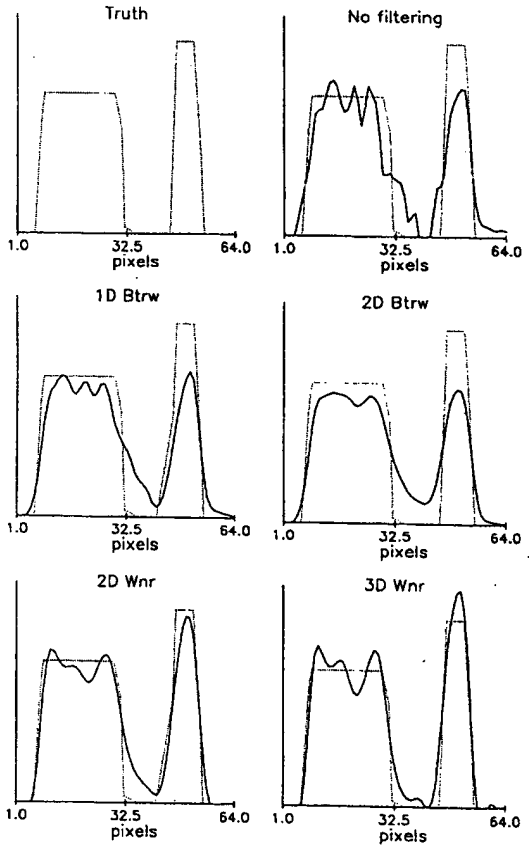

Figure 4. Profiles through the liver and spleen for each of the cases shown in Figure 3. It can be observed that profiles of the slices obtained with the restoration filters are closer to the true profile than those obtained with no processing of the smoothing filters.

TABLE I

Comparison of cold spot contrast, standard deviation in tumor contrast (std. contrast), normalized mean square error (NMSE), and area under the receiver operator characteristic curves obtained for filtered simulated liver spleen study. The abbreviations for the different processing methods are: 1D BTRW - 1D Butterworth, 2D BTRW - 2D Butterworth, 2D WNR - 2D Wiener, and 3D WNR - 3D Wiener.

	1D BTRW	2D BTRW	2D WNR	3D WNR
contrast (%)	16.0	12.4	16.7	25.0
std. contrast	25.0	13.7	15.5	25.7
NMSE (%)	12.8	12.6	7.9	6.0
ROC area	0.75	0.81	0.83	0.82

IV. REFERENCES

[1] M.A. King, R.B. Schwinger, B.C. Penney, P.W. Doherty, and J.A. Bianco, "Digital restoration of indium-111 and iodine-123 images with optimized Metz filters," *J. Nucl. Med.*, vol. 27, pp. 1327-1336, August 1986.

[2] B.C. Penney, M.A. King, and S.J. Glick, "Restoration of combined conjugate images in SPECT: comparison of a new Wiener filter and the image-dependent Metz filter," *IEEE Trans. Nucl. Sci.*, vol. 37, pp. 707-713, April 1990.
[3] S.J. Glick, M.A. King, K. Knesaurek, and K. Burbank,"An investigation of the stationarity of the 3D modulation transfer function of SPECT," *IEEE Trans. Nucl. Sci.*, vol. 36, pp. 973-977, February 1989.
[4] S. Bellini, M. Piacentini, and C. Cafforio, "Compensation of tissue absorption in emission tomography," *IEEE Trans ASSP.*, vol. 27, pp. 213-218, June 1979.
[5] S.J Glick, W.G. Hawkins, M.A. King, B.C. Penney, E.J. Soares, and C. Byrne, "The effect of intrinsic attenuation correction methods on the stationarity of the 3D modulation transfer function of SPECT", *Med. Phys.*, in press.
[6] S.J. Glick, "Restoration filtering of SPECT images," Worcester Polytechnic Institute, Ph.D. dissertation, 1991.
[7] B.C. Penney, S.J. Glick, and M.A. King, "Relative importance of the error sources in Wiener restoration of scintigrams," *IEEE Trans. Med. Imag.*, vol. MI-9, pp. 60-70, March, 1990.
[8] M.T. Madsen, "A method for obtaining an approximate Wiener filter," *Med. Phys.*, vol. 17, pp. 126-130, January 1990.
[9] B.C. Penney, M.A. King, and K. Knesaurek, "A projector back-projector pair which accounts for the two-dimensional depth and distance dependent blurring in SPECT," *IEEE Trans. Nucl. Sci.*, vol. NS-37, pp. 681-687, April, 1990.
[10] K. Knesaurek, M.A. King, S.J. Glick, and B.C. Penney, "A 3-D non-stationary simulation of SPECT imaging," *J. Nucl. Med.*, vol. 30, pp. 881, May, 1989.
[11] S.J. Glick, B.C. Penney, M.A. King, and E.J. Soares, "Three dimensional, post-reconstruction restoration filtering of SPECT images," *J. Nucl. Med.*, vol. 31, pp. 867, May 1990.
[12] R.C. Gonzalez and P. Wintz, *Digital Image Processing*, Addison-Wesley Publishing Co., Reading, MA, 1977.
[13] J. Rahimian, J. Contino, H.F. Corbus, and J.J. Toyua, "Performance index: a method of quantitative evaluation of filters used in clinical SPECT," *Med. Phys.*, vol. 11, pp. 404, May/June 1984.
[14] C.R. Appledorn, B.E. Oppenheim, N.N. Wellman, "Performance measures in the selection of reconstruction filters for SPECT imaging," *J. Nucl. Med.*, vol. 26, pp. P35-36, May 1985.
[15] R.H Huesman, G.T. Gullberg, W.L. Greenberg, and T.F. Budinger, *Donner algorithms for reconstruction tomography*, Publication 214, Lawrence Berkeley Laboratory, Univ. of California, Berkeley, CA, pp. 91-92, 1977.
[16] K.M. Hanson, "Method to evaluate image-recovery algorithms based on task performance," *Proc. SPIE*, vol. 914, pp. 336-343, February 1989.
[17] M.A. King, R.B. Schwinger, B.C. Penney, P. Stritzke, "The design of optimal two-dimensional pre-reconstruction filters for SPECT images," *CAR '87 Computer Assisted Radiology*, Springer-Verlag, pp. 703-707, 1987.
[18] J.P. Rolland, H.H. Barrett, and G.W. Seely, "Quantitative study of deconvolution and display mappings for long-tailed point spread functions," SPIE, vol. 1092, pp. 17-21, 1989.
[19] J.P. Rolland, "Factors influencing lesion detection in medical imaging," University of Arizona, Ph.D. dissertation, 1989.